

# MOF-like supramolecular network of Mn<sub>3</sub> single-molecule magnets formed by extensive $\pi$ – $\pi$ stacking



Tu N. Nguyen, Khalil A. Abboud, George Christou\*

Department of Chemistry, University of Florida, Gainesville, FL 32611-7200, United States

## ARTICLE INFO

### Article history:

Received 14 August 2015

Accepted 19 September 2015

Available online 28 September 2015

Dedicated to Malcolm H. Chisholm on the occasion of his 70th birthday; an outstanding scientist and friend.

### Keywords:

Manganese

Mn/O triangular cluster

Crystal structure

Single-molecule magnet

$\pi$ – $\pi$  stacking

## ABSTRACT

[Mn<sub>3</sub>O(dhb)<sub>3</sub>(mpko)<sub>3</sub>](ClO<sub>4</sub>) (**4**) has been obtained from the carboxylate substitution reaction of triangular [Mn<sub>3</sub>O(O<sub>2</sub>CMe)<sub>3</sub>(mpko)<sub>3</sub>](ClO<sub>4</sub>) (mpkoH = methyl(2-pyridyl)ketone oxime) with 3,5-dihydroxybenzoic acid (dhbH). Complex **4** possesses an equilateral triangle [Mn<sub>3</sub>O]<sup>7+</sup> core with the dhb<sup>–</sup> and mpko<sup>–</sup> ligands on opposite sides of the Mn<sub>3</sub> plane. All dhb<sup>–</sup> and mpko<sup>–</sup> groups are involved in  $\pi$ – $\pi$  stacking interactions with those on neighboring Mn<sub>3</sub> molecules to give a 3-D supramolecular network resembling a metal–organic framework (MOF), with periodic voids resulting from a repeating unit comprising an [Mn<sub>3</sub>]<sub>8</sub> rhombohedron. Variable-temperature, solid-state magnetic susceptibility studies in the 5.0–300 K temperature range reveal the predominance of antiferromagnetic inter-Mn<sub>3</sub> exchange couplings. Alternating current magnetic susceptibility studies on **4** show that the single-molecule magnet (SMM) behavior characteristic of [Mn<sub>3</sub>O(O<sub>2</sub>CR)<sub>3</sub>(mpko)<sub>3</sub>]<sup>+</sup> complexes has been lost. This work demonstrates that constructing MOF-like networks from SMMs by weak interactions is feasible but that even these can introduce significant inter-SMM exchange interactions that weaken or destroy the SMM properties.

© 2015 Elsevier Ltd. All rights reserved.

## 1. Introduction

Metal–organic frameworks (MOFs) are polymeric coordination compounds that are formed by linking together inorganic building blocks, i.e., metal ions or metal clusters, using suitable chosen organic linkers. Different from synthetic inorganic polymers such as silica gel or zeolite, whose structures do not include organic carbon units, MOFs offer high degrees of tunability allowing for tailoring of structural and physicochemical properties. Thus they have emerged as promising materials for a variety of applications such as gas separation and storage, heterogeneous catalysis, drug delivery, biological imaging, battery components, and others [1–6]. Recently, there has been a growing interest in applying MOF chemistry to molecular magnetism to take advantage of the high porosity of these materials and possible host–guest chemistry [7]. The amalgamation of molecular magnetism and supramolecular chemistry presents an important facet of modern inorganic chemistry because such materials have potential in applications that span chemistry, physics, and biology [8]. Several studies have shown that constructing MOFs from magnetic building blocks together with controlling the encapsulation of the species within the frameworks lead to dual- or multifunctional materials [9–13]. Such

studies are providing great encouragement and inspiration to chemists to explore the various fundamental aspects of magnetic MOF development, e.g., to understand the factors that affect the degree of similarity of the magnetic properties of an obtained MOF with those of the monomeric building block, and the sensitivity of the magnetic properties to the identity of the MOF linker group employed, allowing factors to be identified that should be prevented when constructing magnetic MOFs. In this work, we will face such questions in a particular case when a MOF-like network is assembled, using non-covalent interactions, from Mn<sub>3</sub> building blocks that are single-molecule magnets (SMMs).

Single-molecule magnets are individual molecules that function as single-domain nanoscale magnetic particles below their blocking temperature,  $T_B$  [14–18]. For Mn and most 3d transition metal SMMs, this behavior arises from the combination of a large ground-state spin ( $S$ ) and Ising-type magnetoanisotropy (negative zero-field splitting parameter,  $D$ ), which leads to a large (versus  $kT$ ) barrier to magnetization relaxation. SMMs exhibit frequency-dependent out-of-phase ac magnetic susceptibility signals, and hysteresis in a plot of magnetization vs applied dc magnetic field. SMMs have been shown to also display interesting quantum phenomena such as quantum tunneling of magnetization (QTM) [19,20], quantum phase interference [21–23], spin–spin cross relaxation [24], and quantum entanglement [25–27]. Consequently, they have been proposed as qubits for quantum

\* Corresponding author. Tel.: +1 352 392 8314; fax: +1 352 392 8757.

E-mail address: [christou@chem.ufl.edu](mailto:christou@chem.ufl.edu) (G. Christou).

**Table 1**  
Crystallographic data for complex **4**·4MeCN.

Formula <sup>a</sup>	C <sub>48</sub> H <sub>45</sub> ClMn <sub>3</sub> N <sub>9</sub> O <sub>20</sub>
FW (g/mol) <sup>a</sup>	1268.20
Crystal system	Rhombohedral
Space group	R $\bar{3}c$
<i>a</i> = <i>b</i> (Å)	18.6647(12)
<i>c</i> (Å)	60.960(6)
$\gamma$ (°)	120
<i>V</i> (Å <sup>3</sup> )	18392(2)
<i>Z</i>	12
<i>T</i> (K)	100(2)
$\lambda$ (Å) <sup>b</sup>	0.71073
$\rho_{\text{calc}}$ (mg/m <sup>3</sup> )	1.374
$\mu$ (mm <sup>-1</sup> )	0.727
<i>R</i> <sub>1</sub> <sup>c,d</sup>	0.0777
<i>wR</i> <sub>2</sub> <sup>e</sup>	0.2499

<sup>a</sup> Including solvent molecules.

<sup>b</sup> Graphite monochromator.

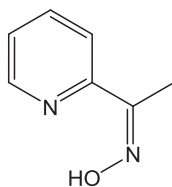
<sup>c</sup>  $I > 2\sigma(I)$ .

<sup>d</sup>  $R_1 = \sum(|F_o| - |F_c|) / \sum|F_o|$ .

<sup>e</sup>  $wR_2 = [\sum[w(F_o^2 - F_c^2)^2] / \sum[w(F_o^2)^2]]^{1/2}$  where  $w = 1 / [\sigma^2(F_o^2) + (m \times p)^2 + n \times p]$ ,  $p = [\max(F_o^2, 0) + 2F_c^2] / 3$ , *m* and *n* are constants.

computation [28–31] and as components in molecular spintronics devices [32,33], which would exploit their quantum tunneling properties.

Linking SMMs into 1-D chains or 2-D sheets is well-known [34,35] but only a few examples have been reported of 3-D MOFs constructed from SMM building-blocks, most of them by employing covalent organic linkers [36–40]. A diamagnetic 3-D mesoporous MOF as a platform to incorporate Mn<sub>12</sub>Ac SMMs was also reported recently [41]. On the other hand, supramolecular networks connected with weak bonds such as hydrogen-bonds or  $\pi$ – $\pi$  stacking are very rare but would be interesting to study further because despite the molecular origin of the magnetic properties of SMMs, in the solid-state even weak exchange couplings can have significant influence on their magnetic properties. The report of supramolecular C–H...Cl hydrogen-bonded pairs of [Mn<sub>4</sub>O<sub>3</sub>Cl<sub>4</sub>(O<sub>2</sub>CET)<sub>3</sub>(py)<sub>3</sub>] (*S* = 9/2) demonstrated such inter-SMM coupling for the first time, leading to identification of exchange-biased QTM steps, quantum superposition states, and quantum entanglement of the two SMMs [25,27,42]. We recently also reported a  $\pi$ – $\pi$  stacked 2-D array of Mn<sub>4</sub> SMMs [43], and to extend our work in this area further, we have now turned our attention to exploring the [Mn<sub>3</sub>O(O<sub>2</sub>CR)<sub>3</sub>(mpko)<sub>3</sub>]<sup>+</sup> (R = Me (**1**), Et (**2**), Ph (**3**); mpkoH = methyl(2-pyridyl)ketone oxime) family of SMMs [44] with spin *S* = 6 as starting points for network



**mpkoH**

formation. Herein, we describe the synthesis, structural characterization, and magnetic properties of a MOF-like supramolecular network formed by the new 3,5-dihydroxybenzoate member of the family.

## 2. Experimental

### 2.1. Synthesis

All preparations were performed under aerobic conditions using materials and solvents as received unless otherwise stated.

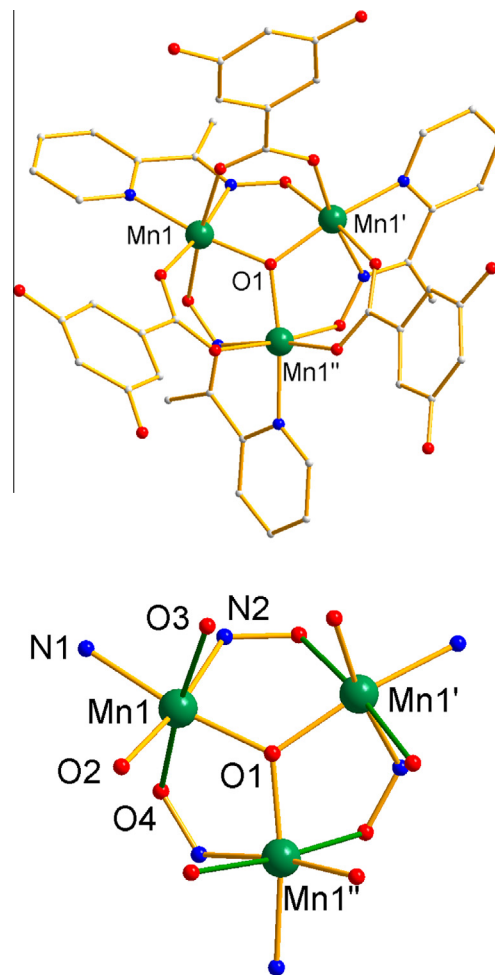


**Fig. 1.** Structure of the cation of **4** (top) and its core (bottom); H atoms have been omitted for clarity. The Mn<sup>III</sup> JT elongation axes are shown as green bonds. Color code: Mn<sup>III</sup> green, O red, N blue, C grey. (Color online.)

**Table 2**  
Selected bond distances (Å) and angles (°) for complex **4**.

Mn1–Mn1' <sup>a</sup>	3.2057(10)
Mn1–O1	1.8747(10)
Mn1–O2	1.925(3)
Mn1–N2	2.009(3)
Mn1–N1	2.022(3)
Mn1–O3	2.185(3)
Mn1–O4	2.197(3)
Mn1–O1–Mn1'	117.52(8)
Mn1–N2–O4–Mn1' <sup>b</sup>	15.10(4)

<sup>a</sup> Prime indicates crystallographic symmetry.

<sup>b</sup> Torsion angle.

**Table 3**  
Bond valence sums (BVS)<sup>a</sup> for the Mn atoms and selected O atoms of **4**.

Atom	Mn <sup>II</sup>	Mn <sup>III</sup>	Mn <sup>IV</sup>	Assignment
Mn1	3.30	<b>3.08</b>	3.16	Mn <sup>III</sup>
O1	2.18			O <sup>2-</sup>

<sup>a</sup> For Mn, the bold value is the one closest to the Mn charge for which it was calculated; the oxidation state is the nearest integer to the bold value. For O, it is non-protonated if its BVS is ~1.8–2.2, mono-protonated if ~1.0–1.4, and doubly-protonated if ~0.2–0.4.

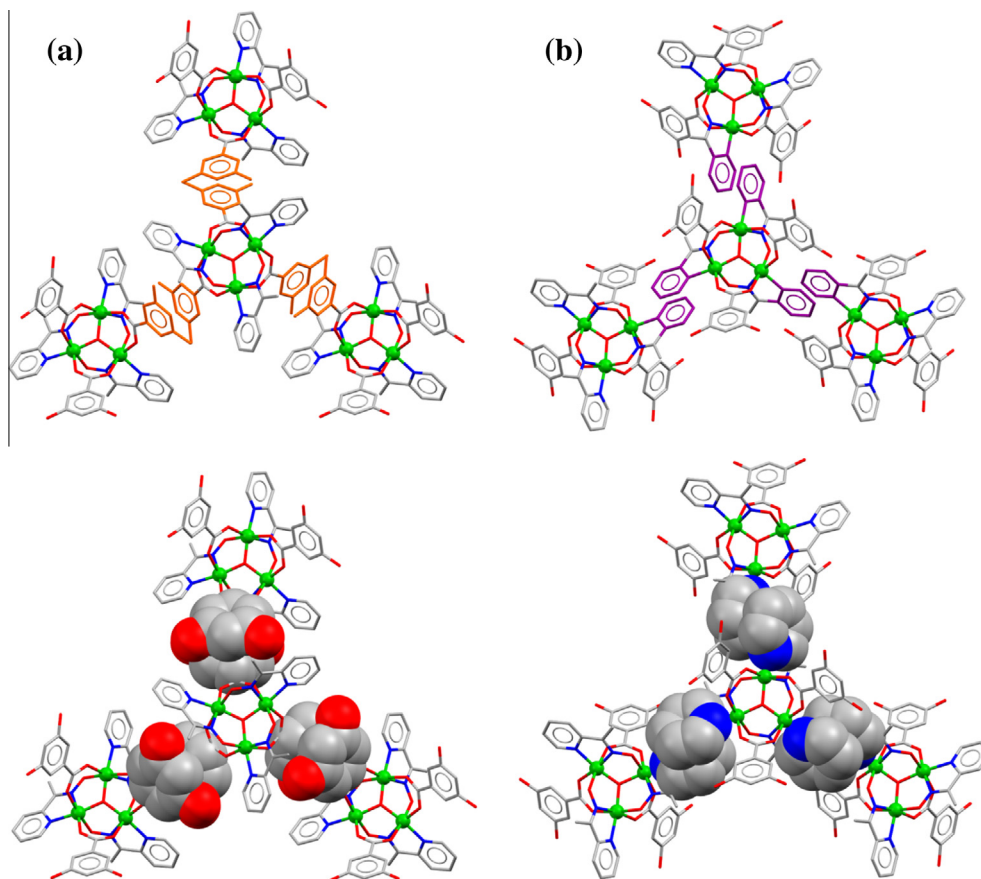


**Fig. 2.** (a)  $\pi$ - $\pi$  stacking of  $\text{dhb}^-$  groups shown as orange stick (top) and space-filling (bottom) representations. (b)  $\pi$ - $\pi$  stacking of  $\text{mpko}^-$  pyridyl groups shown as purple stick (top) and space-filling (bottom) representations. Color code:  $\text{Mn}^{\text{III}}$  green, O red, N blue, C grey. (Color online.)

$[\text{Mn}_3\text{O}(\text{O}_2\text{CMe})_3(\text{mpko})_3](\text{ClO}_4)$  (**1**) was prepared as described elsewhere [44];  $\text{dhbH} = 3,5$ -dihydroxybenzoic acid.

#### 2.1.1. $[\text{Mn}_3\text{O}(\text{dhb})_3(\text{mpko})_3](\text{ClO}_4)$ (**4**)

A brown solution of complex **1** (0.17 g, 0.20 mmol) in MeCN: EtOH (30 mL; 2:1 v/v) was treated with solid  $\text{dhbH}$  (0.092 g, 0.60 mmol), and the solution was stirred overnight at room temperature. Toluene (10 mL) was added and the solvent was removed under vacuum. After three cycles of toluene addition and removal, the residue was dissolved in MeCN (25 mL) and the resulting solution was left undisturbed. X-ray quality crystals of **4**·MeCN slowly formed over one week. The crystals were collected by filtration, washed with  $\text{Et}_2\text{O}$ , and dried in air. The yield was  $\sim 18\%$  based on Mn. *Anal. Calc.* for **4**·2MeCN ( $\text{Mn}_3\text{O}_{20}\text{C}_{46}\text{H}_{42}\text{N}_8\text{Cl}$ ): C, 45.02 (45.37); H, 3.45 (3.53); N, 9.13 (8.85)<sup>1</sup>. Selected IR data (KBr,  $\text{cm}^{-1}$ ): 1603 (s), 1559 (s), 1476 (w), 1384 (s), 1158 (m), 1107 (w), 1046 (w), 1004 (w), 857 (w), 778 (m), 699 (w), 666 (w), 620 (w).

## 2.2. General and physical measurements

Infrared spectra were recorded in the solid state (KBr pellets) on a Nicolet Nexus 670 FTIR spectrometer in the 400–4000  $\text{cm}^{-1}$  range. Elemental analyses (C, H and N) were performed by the in-house facilities of the University of Florida, Chemistry Department. Variable-temperature direct current (dc) and alternating current (ac) magnetic susceptibility data were collected using a

Quantum Design MPMS-XL SQUID magnetometer equipped with a 7 T magnet and operating in the 1.8–300 K range. Samples were embedded in solid eicosane to prevent torquing. Pascal's constants were used to estimate the diamagnetic correction, which were subtracted from the experimental susceptibility to give the molar magnetic susceptibility ( $\chi_M$ ).

#### 2.2.1. X-ray crystallography

Data were collected at 100 K on a Bruker **DUO** diffractometer using Mo  $\text{K}\alpha$  radiation ( $\lambda = 0.71073 \text{ \AA}$ ) and an APEXII CCD area detector. A suitable crystal of **4**·MeCN was attached to the glass fiber using silicone grease and transferred to a goniostat where it was cooled to 100 K for data collection. Raw data frames were read by the program SAINT [45] and integrated using 3-D profiling algorithms. The resulting data were reduced to produce  $hkl$  reflections, their intensities, and estimated standard deviations. The data were corrected for Lorentz and polarization effects, and numerical absorption corrections were applied based on indexed and measured faces. The structure was solved and refined on  $F^2$  in SHELXTL6.1, using full-matrix least-squares refinement cycles. The non-H atoms were refined with anisotropic thermal parameters and all of the H atoms were placed in calculated, idealized positions and refined as riding on their parent atoms. The asymmetric unit contains 1/3  $\text{Mn}_3$  cation and 1/3 perchlorate anion. A total of 269 parameters were included in the final refinement cycle using 4710 reflections (of which 3446 are observed with  $I > 2\sigma(I)$ ) to yield  $R_1$  and  $wR_2$  of 7.77% and 23.57%, respectively. Unit cell data and structure refinement details are listed in Table 1.

<sup>1</sup> Elemental analysis indicates some solvent loss without drying under vacuum.

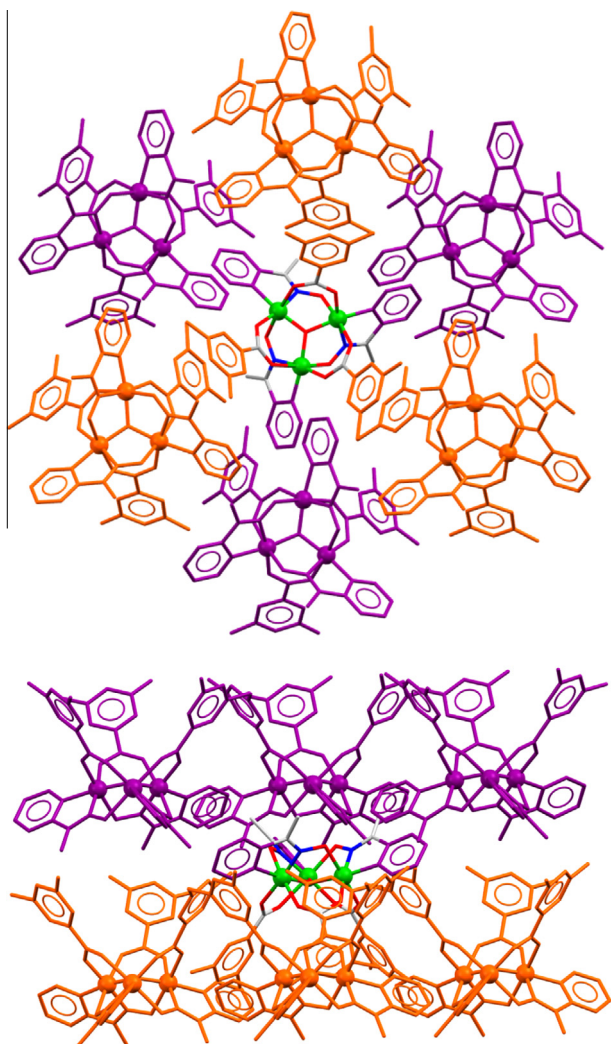
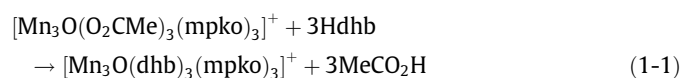


**Fig. 3.** Overall interactions between a  $Mn_3$  cation and six neighboring  $Mn_3$  cations viewed along the  $C_3$  axis (top) and from a side-view (bottom). Color code: orange = interactions via  $dhb^-$  groups; purple = interactions via  $mpko^-$  groups. (Color online.)

### 3. Results and discussion

#### 3.1. Synthesis

The synthesis of complex **4** was carried out by substitution of the acetate groups on complex **1** with  $dhbH$ . Carboxylate substitution is a commonly employed way for the carboxylate ligation to be modified as desired, and it has been especially crucial in allowing targeted modification of SMMs such as the  $Mn_4$  and  $Mn_{12}$  families [46,47]. The only necessary criterion for successful substitution is that the  $M/O$  core is robust and stable to carboxylic acids so that no side-reaction occurs. In the case of **1**, the presence of the firmly bound tridentate pyridyloximate groups of three  $mpko^-$  ligands imparted rigidity and robustness to the molecule during the reaction. The formation of **4** is summarized in Eq. (1-1).



The substitution is an equilibrium whose position depends on the relative acidity of the incoming and outgoing carboxylic acids. Since  $dhbH$  ( $pK_a = 4.04$ ) is a stronger acid than acetic acid ( $pK_a = 4.76$ ), the equilibrium favors the product. Nevertheless, to

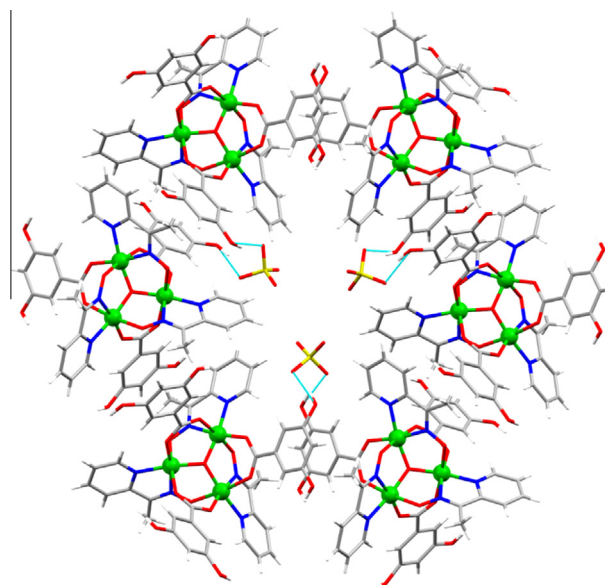


**Fig. 4.** The  $[Mn_3]_6$  ring resulting from aggregation of six  $Mn_3$  cations by  $\pi$ - $\pi$  stacking and H-bonds with the  $ClO_4^-$  anions. Color code:  $Mn^{III}$  green, O red, N dark blue, C grey, Cl yellow. (Color online.)

ensure clean product, toluene was added to allow removal of acetic acid under vacuum as its toluene azeotrope and thus drive the equilibrium to 100% product. The stoichiometric ratio of  $[Mn_3]:dHbH = 1:3$  was used. The low yield (18%) was a consequence of the significant solubility of **4** in MeCN/EtOH, but the product was obtained pure and in a highly crystalline form; we were thus happy to settle for a low yield of such nice material and did not attempt to increase it by concentration or addition of other solvents.

#### 3.2. Structural description of $[Mn_3O(dhb)_3(mpko)_3](ClO_4)$ (**4**)

The labeled structure of complex **4** and its core are shown in Fig. 1. Selected interatomic distances and angles are listed in Table 2. Complex **4** crystallizes in rhombohedral space group  $R\bar{3}c$  with the  $Mn_3$  molecule having crystallographic  $C_3$  symmetry. Its core contains three  $Mn^{III}$  ions in an equilateral triangle bridged by a central  $\mu_3-O^{2-}$  ion. Each edge of the  $Mn_3$  triangle is bridged by a  $\eta^1:\eta^1:\mu-dhb^-$  and a  $\eta^1:\eta^1:\eta^1:\mu-mpko^-$  group, with the pyridyl and oximate nitrogen atoms chelating a  $Mn^{III}$ , forming a five-membered chelate ring. The central  $\mu_3-O^{2-}$  lies slightly above the  $Mn_3$  plane ( $d \sim 0.30$  Å). Overall, the core structure of the cation of **4** is essentially identical to those of the  $[Mn_3O(O_2CR)_3(mpko)_3]^+$  cations of the R = Me (**1**), Pr (**2**), Ph (**3**) analogues. The Mn oxidation states were determined from bond valence sum (BVS) calculations (Table 3), charge balance considerations, and the presence of Jahn–Teller (JT) axial elongations on the  $Mn^{III}$  atoms (Fig. 1, right).

Inspection of the packing in **4** reveals extensive  $\pi$ - $\pi$  stacking interactions ( $\sim 3.4$  Å, well below the  $\pi$ - $\pi$  stacking upper-limit distance of  $\sim 3.7$  Å [48]) between neighboring  $Mn_3$  cations. Each cation  $\pi$ - $\pi$  stacks with three neighboring  $Mn_3$  cations on either side of the  $Mn_3$  plane via the  $dhb^-$  (Fig. 2a) and  $mpko^-$  ligands (Fig. 2b), respectively. Thus, a total of six  $Mn_3$  cations interact with each  $Mn_3$  molecule (Fig. 3). In addition, each  $\pi$ - $\pi$  stacked pair of  $dhb^-$  rings on adjacent cations is also connected by strong H-bonds between  $dhb^-$  OH groups and  $ClO_4^-$  anion O atoms ( $O \cdots O \sim 2.7$  Å); this connects two sets of three  $Mn_3$  cations into a trigonal antiprismatic  $[Mn_3]_6$  aggregate (Fig. 4). As a result of the  $\pi$ - $\pi$  interactions, a 3-D MOF-like network structure is formed (Fig. 5, bottom) with the repeating unit being a  $[Mn_3]_8$  rhombohedron involving  $Mn_3$

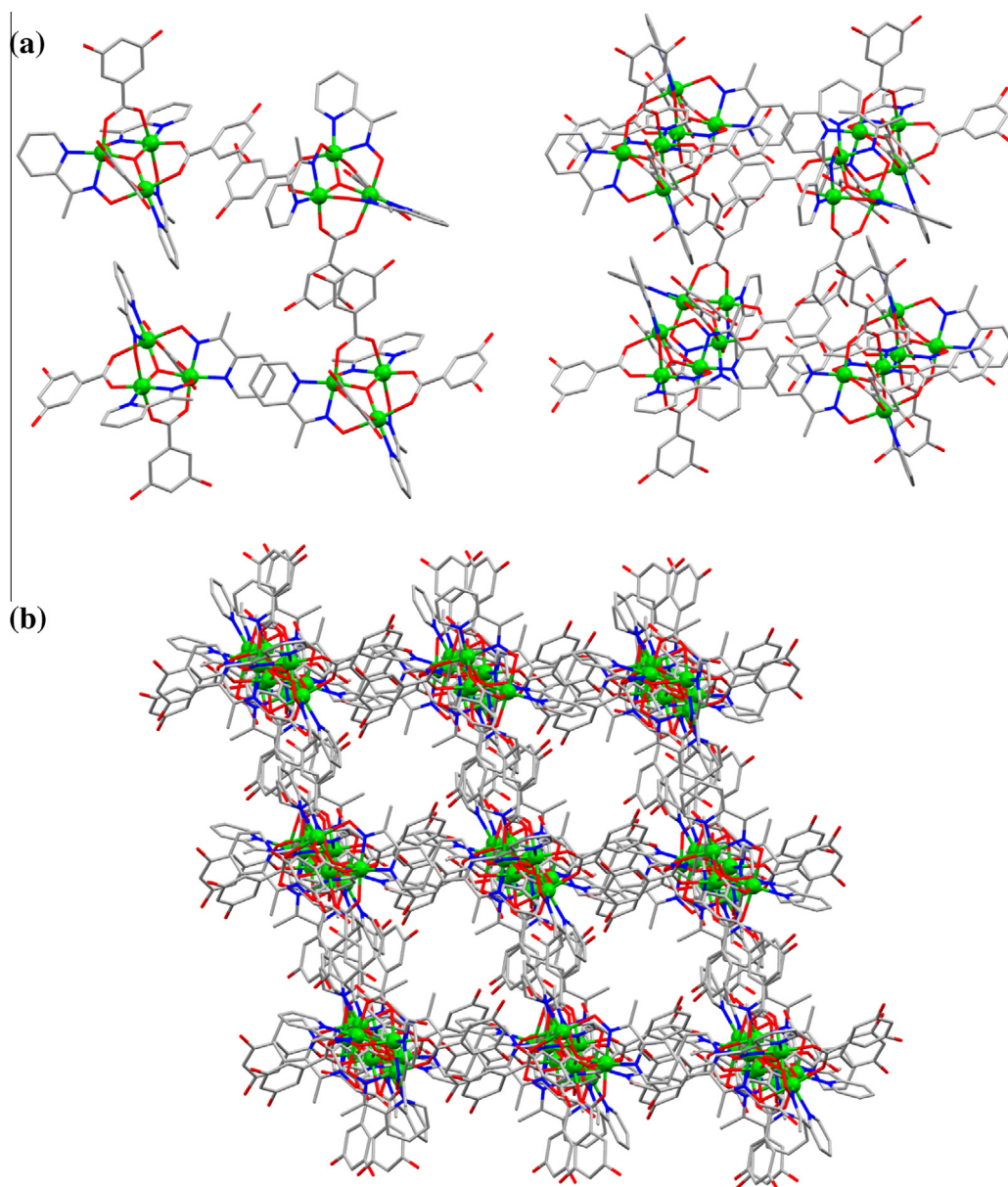


**Fig. 5.** (a) One  $[\text{Mn}_3]_4$  rhombic face of the  $[\text{Mn}_3]_8$  rhombohedron emphasizing the two types of  $\pi$ - $\pi$  stacking (left), and the complete  $[\text{Mn}_3]_8$  rhombohedron (right). (b) A section of the complete 3-D network formed from face-fused  $[\text{Mn}_3]_8$  rhombohedra.

cations lying at the eight vertices (Fig 5a, right). Each rhombic face of the rhombohedron comprises four  $\text{Mn}_3$  cations linked together by a total of four  $\pi$ - $\pi$  interactions, two of which involve  $\text{dhb}^-$  ligands and two involve  $\text{mpko}^-$  ligands (Fig 5a, left). The complete 3-D network is then formed by face-fused rhombohedra (Fig 5b).

The  $[\text{Mn}_3]_8$  rhombohedron encloses a void with a solvent accessible volume of  $\sim 640 \text{ \AA}^3$  ( $0.64 \text{ nm}^3$ ) (probe radius  $1.6 \text{ \AA}$ , grid spacing  $0.5 \text{ \AA}$ ). Of interest with all MOF and MOF-like frameworks containing sizeable voids is what guest molecules might be present in those voids. In **4-MeCN**, the rhombohedron is large enough for encapsulation of eight MeCN guest molecules, with this  $[\text{MeCN}]_8$  collection packing in an interesting way to give a triangular-face-bicapped trigonal antiprismatic assembly of  $S_6$  crystallographic symmetry (Fig 6); each  $[\text{MeCN}]_3$  triangle has the MeCN molecules arranged like the blades of a propeller. This suggests that a variety of other small organic or inorganic molecules could also be accommodated as guests. This host-guest chemistry provides another motivation for ongoing work since many examples of MOFs

encapsulating polar guest molecules such as ethanol, methanol or water have been found to exhibit ferroelectric responses [9,49–51].

### 3.3. Magnetochemistry

#### 3.3.1. DC Magnetic susceptibility studies

The  $\text{Mn}_3$  cation structure of **4** is very similar to those of  $[\text{Mn}_3\text{O}(\text{O}_2\text{CR})_3(\text{mpko})_3]^+$  ( $\text{R} = \text{Me}$  (**1**),  $\text{Pr}$  (**2**),  $\text{Ph}$  (**3**)) complexes. The latter have been established as having ferromagnetic (F) exchange couplings between the  $\text{Mn}^{\text{III}}$  atoms as a result of core distortions caused by binding of the  $\text{mpko}^-$  chelates, such as the non-zero oximate  $\text{Mn-N-O-Mn}$  torsion angles in the range  $9.6$ – $15.4^\circ$ , leading to spin  $S = 6$  ground states for the complexes [44]. Complex **4**, with a similar structure to **1–3** including torsion angles of  $15.1^\circ$  (Table 2), is therefore also expected to exhibit F coupling and have an  $S = 6$  ground state.

Variable-temperature, direct current (dc) magnetic susceptibility ( $\chi_M$ ) measurements were performed on dried polycrystalline

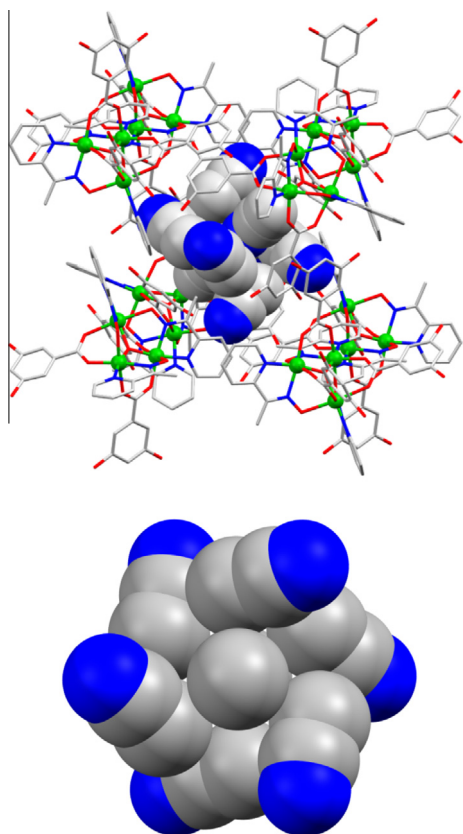


**Fig. 6.** (top) One  $[\text{Mn}_3]_8$  rhombohedron showing the eight MeCN guest molecules in space-filling representation, and (bottom) the  $[\text{MeCN}]_8$  solvent assembly looking down the  $S_6$  axis. Color code: Mn<sup>III</sup> green, O red, N blue, C grey. (Color online.)

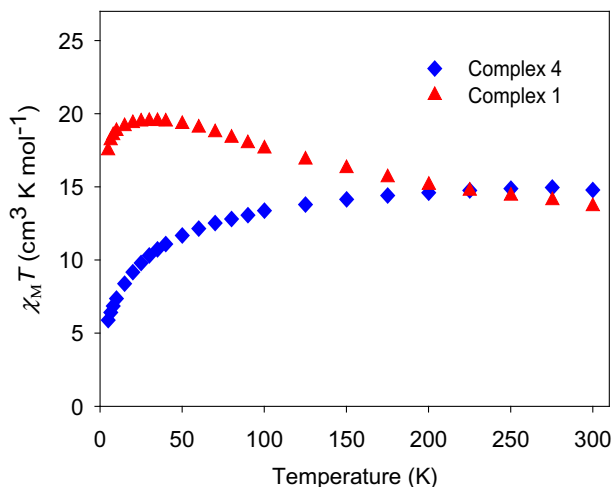


**Fig. 7.** Plot of  $\chi_M T$  vs.  $T$  for dried microcrystalline **1** and **4.2MeCN** in a 1000 kG (0.1 T) dc field.

samples of **4.2MeCN** in an applied field of 1000 G (0.10 T) in the 5.0–300 K temperature range. The samples were restrained in eicosane to prevent torquing. The obtained data are shown as a  $\chi_M T$  versus  $T$  plot in Fig. 7, which also shows the data for **1** for comparison.  $\chi_M T$  for **4** steadily decreases from 14.78  $\text{cm}^3 \text{K mol}^{-1}$  at 300 K to 5.89  $\text{cm}^3 \text{K mol}^{-1}$  at 5.0 K. The 300 K value is larger than the spin-only ( $g=2$ ) value for three Mn<sup>III</sup> non-interacting ions (9.00  $\text{cm}^3 \text{K mol}^{-1}$ ), which indicates **F** intra- $\text{Mn}_3$  interactions, as expected from the structural similarity to **1–3**. However, the

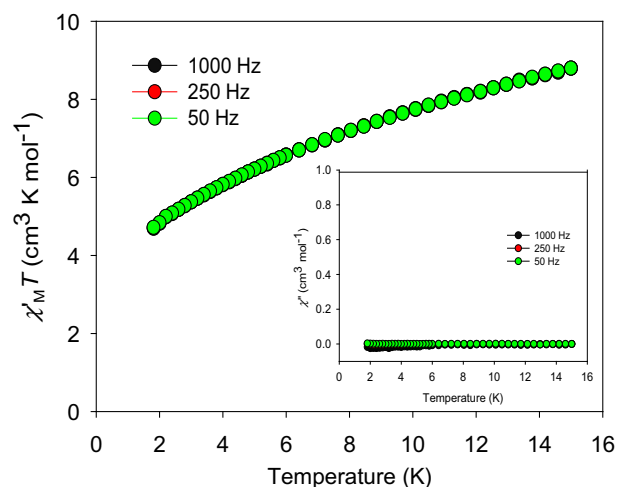


**Fig. 8.** Plot of ac susceptibility in-phase ( $\chi'_M T$ ) vs.  $T$  and (inset) out-of-phase ( $\chi''_M$ ) vs.  $T$  data for dried microcrystalline **4.2MeCN** at the indicated frequencies.

overall  $\chi_M T$  versus  $T$  profile for **4** is then very different from that for **1–3**, which increase with decreasing temperature;  $\chi_M T$  for **4** instead decreases with decreasing temperature. We assign this to antiferromagnetic (**AF**) exchange interactions between neighboring  $\text{Mn}_3$  units as a result of the many inter- $\text{Mn}_3$   $\pi$ - $\pi$  stacking interactions that each  $\text{Mn}_3$  undergoes in this 3-D network. In the literature,  $\pi$ - $\pi$  stacking has been identified as leading to either **F** [52,53] or **AF** interactions between spin-carriers [44,54]. However, **F** interactions by  $\pi$ - $\pi$  stacking are rare because they occur when an organic radical is involved, which has been explained by either a McConnell I spin-polarization mechanism or a McConnell II charge-transfer mechanism [55,56]. In **4**, the  $\pi$ - $\pi$  stacking does not involve a radical and thus is expected to lead to inter- $\text{Mn}_3$  **AF** interactions. They will be weak, but they are many, and since there is also expected to be significant spin density in the  $\pi$ -systems, especially the  $\text{mpko}^-$  pyridyl ring, they will be of significant strength relative to the intra- $\text{Mn}_3$  interactions, and thus lead to the observed  $\chi_M T$  versus  $T$  profile.

### 3.3.2. AC magnetic susceptibility studies

Alternating current (ac) magnetic susceptibility measurements were performed on **4.2MeCN** in the 1.8–15 K range in a 3.5 G ac field with oscillation frequencies of 50–1000 Hz. The in-phase ( $\chi'_M$ , as  $\chi'_M T$  versus  $T$ ) and out-of-phase ( $\chi''_M$  versus  $T$ ) data are shown in Fig. 8. The in-phase  $\chi'_M T$  versus  $T$  for **4** steadily decreases with decreasing temperature, consistent with the trend observed in the dc  $\chi_M T$  versus  $T$  plot. The members of the  $[\text{Mn}_3\text{O}(\text{O}_2\text{CR})_3(\text{mpko})_3]^+$  family are well-known for their SMM behavior, which is manifested as a peak in the out-of-phase  $\chi''_M$  versus  $T$  plot indicating that the magnetic moment vector of the molecule cannot relax (reorient) fast enough to keep in-phase with the oscillating ac field. However, no out-of-phase  $\chi''_M$  signal was detected for **4** above 1.8 K, the limit of our SQUID magnetometer, indicating at the very least that the inter- $\text{Mn}_3$  exchange coupling has greatly diminished the SMM properties of the different  $\text{Mn}_3$  units.

## 4. Conclusions

3,5-Dihydroxybenzoic acid has been successfully used in the synthesis of a new member of the  $[\text{Mn}_3\text{O}(\text{O}_2\text{CR})_3(\text{mpko})_3]^+$  family. Compound **4** possesses a similar  $\text{Mn}_3$  core structure to previous members of this family but it exhibits extensive inter- $\text{Mn}_3$   $\pi$ - $\pi$  stacking involving  $\text{dhb}^-/\text{dhb}^-$  interactions between dihydroxyphenyl rings, and  $\text{mpko}^-/\text{mpko}^-$  interactions between pyridyl

rings. These extensive interactions lead to the formation of a 3-D MOF-like network with rhombohedral repeating units comprising eight  $Mn_3$  units at the vertices. It is interesting to note that the  $[Mn_3O(O_2CPh)_3(mpko)_3]^+$  cation of **3** was previously found not to exhibit this inter- $Mn_3$   $\pi$ - $\pi$  stacking even though it differs from **4** only in the benzoate substituents, pointing to the importance of the two 3,5-dihydroxy substituents of dhhH to the solid-state structure. As a consequence of the 3-D network, there are many inter- $Mn_3$  AF interactions, which greatly decrease or destroy completely the SMM properties of **4** versus previous members of this family even though the intra- $Mn_3$  coupling is still F. The present work thus demonstrates that even weak inter-SMM  $\pi$ - $\pi$  stacking interactions can seriously damage SMM properties if there are enough of them, and thus great care is needed to minimize all sources of significant inter-SMM exchange interactions in attempting to construct MOF or MOF-like 3-D networks of SMMs to take advantage in potential magnetic applications of the resulting voids that their structure forms.

### Acknowledgments

This work was supported by the National Science Foundation (CHE-1410394). T.N.N. thanks the Vietnam Education Foundation for a fellowship.

### Appendix A

CCDC 1417784 contains the supplementary crystallographic data for **4**-MeCN. These data can be obtained free of charge via <http://www.ccdc.cam.ac.uk/conts/retrieving.html> or from the Cambridge Crystallographic Data Centre, 12 Union Road, Cambridge CB2 1EZ, UK; fax: (+44) 1223-336-033; or e-mail: deposit@ccdc.cam.ac.uk.

### References

- [1] A.U. Czaja, N. Trukhan, U. Müller, *Chem. Soc. Rev.* 38 (2009) 1284.
- [2] Z. Chen, K. Adil, L.J. Weselinski, Y. Belmabkhout, M. Eddaoudi, *J. Mater. Chem. A* 3 (2015) 6276.
- [3] J. Liu, L. Chen, H. Cui, J. Zhang, L. Zhang, C.-Y. Su, *Chem. Soc. Rev.* 43 (2014) 6011.
- [4] R.C. Huxford, J.D. Rocca, W. Lin, *Curr. Opin. Chem. Biol.* 14 (2010) 262.
- [5] A. Foucault-Collet, K.A. Gogick, K.A. White, S. Villette, A. Pallier, G. Collet, C. Kieda, T. Li, S.J. Geib, N.L. Rosi, S. Petoud, *Proc. Natl. Acad. Sci. U.S.A.* 110 (2013) 17199.
- [6] F. Zou, X. Hu, Z. Li, L. Qie, C. Hu, R. Zeng, Y. Jiang, Y. Huang, *Adv. Mater.* 26 (2014) 6622.
- [7] M. Kurmoo, *Chem. Soc. Rev.* 38 (2009) 1353.
- [8] A.D. Katsenis, E.K. Brechin, G.S. Papaefstathiou, in: L.R. MacGillivray, C.M. Lukehart (Eds.), *Metal–Organic Framework Materials*, John Wiley and Sons, UK, 2014.
- [9] H.B. Cui, Z.M. Wang, K. Takahashi, Y. Okano, H. Kobayashi, A. Kobayashi, *J. Am. Chem. Soc.* 128 (2006) 15074.
- [10] P. Jain, V. Ramachandran, R.J. Clark, H.D. Zhou, B.H. Toby, N.S. Dalal, H.W. Kroto, A.K. Cheetham, *J. Am. Chem. Soc.* 131 (2009) 13625.
- [11] Y. Tian, A. Stroppa, Y. Chai, L. Yan, S. Wang, P. Barone, S. Picozzi, Y. Sun, *Sci. Rep.* 4 (2014) 6062.
- [12] J. Ferrando-Soria, H. Khajavi, P. Serra-Crespo, J. Gascon, F. Kapteijn, M. Julve, F. Lloret, J. Pasán, C. Ruiz-Pérez, Y. Journaux, E. Pardo, *Adv. Mater.* 24 (2012) 5625.
- [13] A. Polyakov, A.H. Arkenbout, J. Baas, G.R. Blake, A. Meetsma, A. Caretta, P.H.M. van Loosdrecht, T.T.M. Palstra, *Chem. Mater.* 24 (2012) 133.
- [14] R. Sessoli, D. Gatteschi, A. Caneschi, M.A. Novak, *Nature* 365 (1993) 141.
- [15] R. Sessoli, H.L. Tsai, A.R. Schake, S. Wang, J.B. Vincent, K. Folting, D. Gatteschi, G. Christou, D.N. Hendrickson, *J. Am. Chem. Soc.* 115 (1993) 1804.
- [16] G. Christou, D. Gatteschi, D.N. Hendrickson, R. Sessoli, *MRS Bull.* 25 (2000) 66.
- [17] G. Christou, *Polyhedron* 24 (2005) 2065.
- [18] R. Bagai, G. Christou, *Chem. Soc. Rev.* 38 (2009) 1011.
- [19] J.R. Friedman, M.P. Sarachik, J. Tejada, R. Ziolo, *Phys. Rev. Lett.* 76 (1996) 3830.
- [20] L. Thomas, L. Lioni, R. Ballou, D. Gatteschi, R. Sessoli, B. Barbara, *Nature* 383 (1996) 145.
- [21] W. Wernsdorfer, R. Sessoli, *Science* 284 (1999) 133.
- [22] W. Wernsdorfer, M. Soler, G. Christou, D.N. Hendrickson, *J. Appl. Phys.* 91 (2002) 7164.
- [23] W. Wernsdorfer, N.E. Chakov, G. Christou, *Phys. Rev. Lett.* 95 (2005) 037203.
- [24] W. Wernsdorfer, S. Bhaduri, R. Tiron, D.N. Hendrickson, G. Christou, *Phys. Rev. Lett.* 89 (2002) 197201.
- [25] S. Hill, R.S. Edwards, N. Aliaga-Alcalde, G. Christou, *Science* 302 (2003) 1015.
- [26] A. Wilson, S. Hill, R.S. Edwards, N. Aliaga-Alcalde, G. Christou, *AIP Conf. Proc.* 850 (2006) 1141.
- [27] R. Tiron, W. Wernsdorfer, D. Foguet-Albiol, N. Aliaga-Alcalde, G. Christou, *Phys. Rev. Lett.* 91 (2003) 227203.
- [28] M.N. Leuenberger, D. Loss, *Nature* 410 (2001) 789.
- [29] B. Zhou, R. Tao, S.-Q. Shen, J.-Q. Liang, *Phys. Rev. A* 66 (2002) 010301(R).
- [30] M. Affronte, F. Troiani, A. Ghirri, A. Candini, M. Evangelisti, V. Corradini, S. Carretta, P. Santini, G. Amoretti, F. Tuna, G. Timco, R.E.P. Winpenny, *J. Phys. D Appl. Phys.* 40 (2007) 2999.
- [31] R. Vincent, S. Klyatskaya, M. Ruben, W. Wernsdorfer, F. Balestro, *Nature* 488 (2012) 357.
- [32] L. Bogani, W. Wernsdorfer, *Nat. Mater.* 7 (2008) 179.
- [33] K. Katoh, H. Ishiki, T. Komeda, M. Yamashita, *Chem. Asian J.* 7 (2012) 1154.
- [34] I. Jeon, R. Clérac, *Dalton Trans.* 41 (2012) 9569.
- [35] H. Miyasaka, K. Nakata, L. Lecren, C. Coulon, Y. Nakazawa, T. Fujisaki, K. Sugiura, M. Yamashita, R. Clérac, *J. Am. Chem. Soc.* 128 (2006) 3770.
- [36] K.W. Galloway, M. Schmidtman, J. Sanchez-Benitez, K.V. Kamenev, W. Wernsdorfer, M. Murrie, *Dalton Trans.* 39 (2010) 4727.
- [37] H. Miyasaka, K. Nakata, K. Sugiura, M. Yamashita, R. Clerac, *Angew. Chem., Int. Ed.* 43 (2004) 707.
- [38] H.-L. Tsai, C.-I. Yang, W. Wernsdorfer, S.-H. Huang, S.-Y. Jhan, M.-H. Liu, G.-H. Lee, *Inorg. Chem.* 51 (2012) 13171.
- [39] E.E. Moushi, T.C. Stamatatos, W. Wernsdorfer, V. Nastopoulos, G. Christou, A.J. Tasiopoulos, *Angew. Chem., Int. Ed.* 45 (2006) 7722.
- [40] X. Yi, G. Calvez, C. Daiguebonne, O. Guillou, K. Bernot, *Inorg. Chem.* 54 (2015) 5213.
- [41] D. Aulakh, J.B. Pyser, X. Zhang, A.A. Yakovenko, K.R. Dunbar, M. Wriedt, *J. Am. Chem. Soc.* 137 (2015) 9254.
- [42] W. Wernsdorfer, N. Aliaga-Alcalde, D.N. Hendrickson, G. Christou, *Nature* 416 (2002) 406.
- [43] T.N. Nguyen, K.A. Abboud, G. Christou, *Polyhedron* 66 (2013) 171.
- [44] T.C. Stamatatos, D. Foguet-Albiol, S.-C. Lee, C.C. Stoumpos, C.P. Raptopoulou, A. Terzis, W. Wernsdorfer, S. Hill, S.P. Perlepes, G. Christou, *J. Am. Chem. Soc.* 129 (2007) 9484.
- [45] SHELXTL6, Bruker-AXS, Madison, Wisconsin, USA, 2008.
- [46] M.W. Wemple, H.-L. Tsai, K. Folting, D.N. Hendrickson, G. Christou, *Inorg. Chem.* 32 (1993) 2025.
- [47] H.J. Eppley, H.-L. Tsai, N. de Vries, K. Folting, G. Christou, D.N. Hendrickson, *J. Am. Chem. Soc.* 117 (1995) 301.
- [48] C. Janiak, *J. Chem. Soc., Dalton Trans.* (2000) 3885.
- [49] H.B. Cui, K. Takahashi, Y. Okano, Z.M. Wang, H. Kobayashi, A. Kobayashi, *Angew. Chem., Int. Ed.* 44 (2005) 6508.
- [50] H.B. Cui, B. Zhou, L.S. Long, Y. Okano, H. Kobayashi, A. Kobayashi, *Angew. Chem., Int. Ed.* 47 (2008) 3376.
- [51] W. Zhang, R.-G. Xiong, *Chem. Rev.* 112 (2012) 1163.
- [52] L.-L. Li, K.-J. Lin, C.-J. Ho, C.-P. Sun, H.-D. Yang, *Chem. Commun.* (2006) 1286.
- [53] Y.-H. Chi, L. Yu, J.-M. Shi, Y.-Q. Zhang, T.-Q. Hu, G.-Q. Zhang, W. Shi, P. Cheng, *Dalton Trans.* 40 (2011) 1453.
- [54] M. Vázquez, A. Taglietti, D. Gatteschi, L. Sorace, C. Sangregorio, A.M. González, M. Maniero, R.M. Pedrido, M.R. Bermejo, *Chem. Commun.* (2003) 1840.
- [55] K. Yoshizawa, R. Hoffmann, *J. Am. Chem. Soc.* 117 (1995) 6921.
- [56] J.S. Miller, A.J. Epstein, *J. Am. Chem. Soc.* 109 (1987) 3850.